Open Access

Research Article

PRNANO

Precis. Nanomed. 2018;1(3):173-182.

ANDOVER HOUSE

Nanoparticle-Encapsulated Doxorubicin Demonstrates Superior Tumor Cell Kill in Triple Negative Breast Cancer Subtypes Intrinsically Resistant to Doxorubicin

Aimee E. Krausz[1#], Brandon L. Adler[1#], Joy Makdisi[1], David Schairer[1], Jamie Rosen[1], Angelo Landriscina[1], Mahantesh Navati[2], Alan Alfieri[2], Joel M. Friedman[2], Joshua D. Nosanchuk[3], Alicia Rodriguez-Gabin[4], Kenny Q Ye[5], Hayley M. McDaid[4,6*], and Adam J. Friedman[1,2,7 *]

[1]Division of Dermatology, Department of Medicine, [2]Department of Physiology and Biophysics, [3]Department of Microbiology & Immunology, [4]Department of Molecular Pharmacology, [5]Department of Epidemiology and Population Health, [6]Department of Medicine (Oncology), Albert Einstein College of Medicine, Bronx, New York, USA, [7]Department of Dermatology, George Washington School of Medicine, Washington, DC, USA

[#]These authors contributed equally to this work
[*]Co-senior authorship

Submitted: July 18, 2018 Accepted: October 22, 2018; Posted October 27, 2018

Abstract

The effect of size and release kinetics of doxorubicin-nanoparticles on anti-tumor efficacy was evaluated in a panel of human cancer cell lines, including triple-negative breast cancer (TNBC) cells that frequently demonstrate resistance to doxorubicin. Different nano-formulations of sol-gel-based Doxorubicin containing nanoparticles were synthesized. Increased cell kill in chemorefractory triple-negative breast cancer cells was associated with the smallest size of nanoparticles and the slowest release of Dox. Modeling of dose-response parameters in Dox-sensitive versus Dox-resistant lines demonstrated increased E_{Max} and area under the curve in Dox-resistant mesenchymal TNBC cells, implying potentially favorable activity in this molecular subtype of breast cancer. Mesenchymal TNBC cells demonstrated a high rate of fluorescent bead uptake suggestive of increased endocytosis, which may partially account for the enhanced efficacy of Dox-np in this subtype. Thus, manipulation of size and release kinetics of this nanoparticle platform is associated with enhanced dose-response metrics and tumor cell kill in therapeutically recalcitrant TNBC cell models. This platform is easily customizable and warrants further exploration.

Keywords:

- Experimental therapeutics
- Nanoparticles
- Triple-negative breast cancer
- Doxorubicin
- Drug resistance
- Dose-response relationship

Abbreviations:

- pCR: Pathologic Complete Response
- TNBC: Triple-Negative Breast Cancer
- AUC: Area under the curve

[*] Corresponding Authors: Adam J. Friedman, MD. Department of Dermatology, George Washington School of Medicine and Health Sciences, 2150 Pennsylvania Avenue NW, Washington, DC 20037. Phone: 202-741-2600; E-mail: ajfriedman@mfa.gwu.edu.

Hayley McDaid, Ph.D. Department of Medicine (Oncology), Forchheimer 249B, 1300 Morris Park Avenue, Albert Einstein College of Medicine, Bronx, NY 10461. Phone: 718-430-8829; E-mail: hayley.mcdaid@einstein.yu.edu

- Dox: Doxorubicin
- Dox-np: Doxorubicin-Nanoparticles

Purpose and Rationale

The purpose of this study was to synthesize and characterize a nanoparticle carrier for doxorubicin (Dox) and evaluate its biologic activity against a range of human cancer cell lines, focusing on TNBC in particular. Our goal was to investigate the pre-clinical anti-tumor activity of Dox-np relative to the parent drug.

Introduction

Doxorubicin, is a well-known anthracycline used primarily in combination chemotherapy for numerous malignancies, notably breast cancer, particularly triple-negative breast cancer (TNBC). The majority of TNBC patients receive a combination of taxane, doxorubicin and cyclophosphamide (TAC), as preoperative neoadjuvant chemotherapy, of which 25–45% achieve pathologic complete response (pCR) and have excellent long-term prognosis (1). Patients who fail TAC have poor prognosis with limited post-operative treatment options available (2). Response to TAC is predominately influenced by the molecular subtype of TNBC (3-5) of which mesenchymal (M) and BL2 tumors have the poorest response and long-term survival due to metastatic biology (2, 4), highlighting an unmet clinical need.

Encapsulation of Dox in a biocompatible nanoparticle platform could expand its narrow therapeutic index (6), enabling slow and sustained release of contents. This has the potential to limit toxicity since the theoretical maximum amount of drug is never in circulation at one time. The most well-known approach to nanoencapsulation of Dox is liposomal doxorubicin (Doxil®), FDA-approved in 1995 for Kaposi's sarcoma. Despite proven clinical superiority and improved tolerability of liposomal doxorubicin, unique adverse events emerged with use (7). In an attempt to further refine Dox delivery, we utilized a sol-gel polymerization technique to create silane composite nanoparticles (8, 9). The platform was modified from a sol-gel-based protocol shown to successfully incorporate a range of therapeutic agents, including amphotericin (10) and sildenafil (11). These particles are formed from amorphous silicon oxide materials that polymerize into a highly structured porous lattice. The large surface area allows for greater drug loading as compared to liposomes (12), and the pore size distribution can be modified to alter the release rate of the encapsulated drug (13). Here we describe their synthesis and enhanced anti-cancer activity, relative to Dox, in cancer cell lines.

Table 1: Dox-np Synthesized with Varying Concentrations of methanol

0% MeOH nanoparticles	40% MeOH nanoparticles	60% MeOH nanoparticles	80% MeOH nanoparticles	100% MeOH nanoparticles
22 mL Tris (50mM)	12.4 mL Tris (50 mM)	7.6 mL Tris (50mM)	2.8 mL Tris (50 mM)	24 mL methanol
1.5 mL chitosan (5mg/ml)	9.6 mL methanol	14.4 mL methanol	19.2 mL methanol	1.5 mL chitosan
1.5 ml PEG 400	1.5 ml chitosan	1.5 ml chitosan	1.5 ml chitosan	1.5 ml PEG 400
2 mL adriamycin (2mg/ml)	1.5 mL PEG 400	1.5 mL PEG 400	1.5 mL PEG 400	2 mL adriamycin (2mg/ml)
3 mL TMOS	2 mL adriamycin (2mg/mL)	2 mL adriamycin (2mg/mL)	2 mL adriamycin (2mg/mL)	3 mL TMOS
0.6 mL HCl (1mM)	3 mL TMOS	3 mL TMOS	3 mL TMOS	0.6 mL HCl (1mM)
	0.6 mL HCl (1mM)	0.6 mL HCl	0.6 mL HCl (1mM)	

In the polymerization phase, the percent concentration of methanol was increased between different samples. 0%, 40%, 60%, 80% and 100% methanol content correspond to Dox-np (A0), (A40), (A60), (A80), and (A100), respectively. See methods for additional detail.

Materials and Methods

Synthesis of Dox nanoparticles (Dox-np)

Clinical grade doxorubicin hydrochloride solution (2 mg/mL) was obtained from Pfizer (New York, NY). A hydrogel/glass composite incorporating Dox as the active component was produced as follows: Tetramethyl orthosilicate (TMOS) was hydrolyzed by adding HCl, followed by 20-minute sonication in an ice water bath. The mixture was refrigerated at 4°C until monophasic. Subsequently, different ratios of Tris-buffered saline and methanol were combined with chitosan, polyethylene glycol, doxorubicin (2 mg/mL), and TMOS-HCl to induce sample polymerization overnight at 4°C (see Table 1 for quantities).

The percent concentration of methanol utilized in Dox-np synthesis was 0%, 40%, 60%, and 80% (represented as Dox-np A0, A40, A60, A80). The hydrogel was subsequently lyophilized at ~200 mTorr for 48–72 hours and the resultant powder processed in a ball mill for ten 30-minute cycles to achieve smaller size and more uniform distribution. Control nanoparticles (control-np) were synthesized identically but without the incorporation of Dox.

(See Supplemental Information for additional methods.)

Results

Dox-np Diameter Characterization

Different variants of Dox-np were synthesized by changing the percent concentration of methanol in the gel phase (Table 1). However, once lyophilized, methanol was removed from the final product, abrogating potential cytotoxicity. The change in size of Dox-np as a function of initial methanol content was determined using dynamic light scattering. Imaging of Dox-np with a scanning electron microscope exhibited a distinct spherical structure with an irregular surface morphology, as shown in Figure 1A. The most significant differences were observed with the Dox-np (A0) and (A80), with an average diameter of 118.6 and 103.4 nm, respectively (Figure 1B).

Dox-np Release Profile

The amount of encapsulated Dox based on release in DMSO was calculated to be 14.5±0.35 ug/ml. The effect of temperature on the release profile of Dox-np was assessed by measuring the spectrophotometric absorbance of a Dox-np solution over time at both 4 and 37°C. Temperatures were selected to simulate storage and in vivo conditions, respectively.

At 4 °C, Dox-np (A0) immediately released 24.6% of encapsulated Dox in solution (t=0 hours) with no further release over 48 hours. In comparison, Dox-np (A80) initially released 11.9% with no further release over time (Figure 1C).

Increasing the temperature to 37°C prompted the continuous release of Dox from the porous matrix in a controlled manner (Figure 1D). The curve for both nano-formulations was characterized by an initial accelerated release from t=0 until t=6 hours, followed by a gradual increase until steady state was reached at 24 hours. Dox-np (A80) had a slower rate of release compared to Dox-np (A0), with lower maximum release after 48 hours. At t=0 hours, Dox-np (A0) released 37.5%, increasing to 60% at 6 hours and reaching a steady state by 24 hours of 68.3%. In comparison, at t=0 Dox-np (A80) released 17.2%, increasing to 31.7% at 6 hours and reaching a steady state by 24 hours of 44.1% release. Since, Dox-np (A80) had a slower release curve compared to Dox-np (A60) and (A40 – not shown). Future cell-based experiments focused mainly on A0 and A80.

Overall, the addition of methanol during Dox-np synthesis correlated with both decreased particle size, and slower initial and maximal release of encapsulated Dox, relative to Dox-np synthesized in the absence of methanol (A0).

Anti-Tumor Efficacy of Dox-np In Cells

We evaluated in-cell activity using multiparametric dose-response modeling in a panel of genetically diverse cancer cell lines. This approach generates metrics to facilitate robust comparison of Dox versus Dox-np using area under the curve (AUC), E_{Max} and EC_{50} as read outs of anti-cancer activity (14). Although EC_{50} is a commonly used metric of potency, it usually reflects a dose that suppresses proliferation. Dose-response curves for all cell lines indicated substantial variation between Dox, Dox-np (A0) and Dox-np (A80), as shown in Figure 2A.

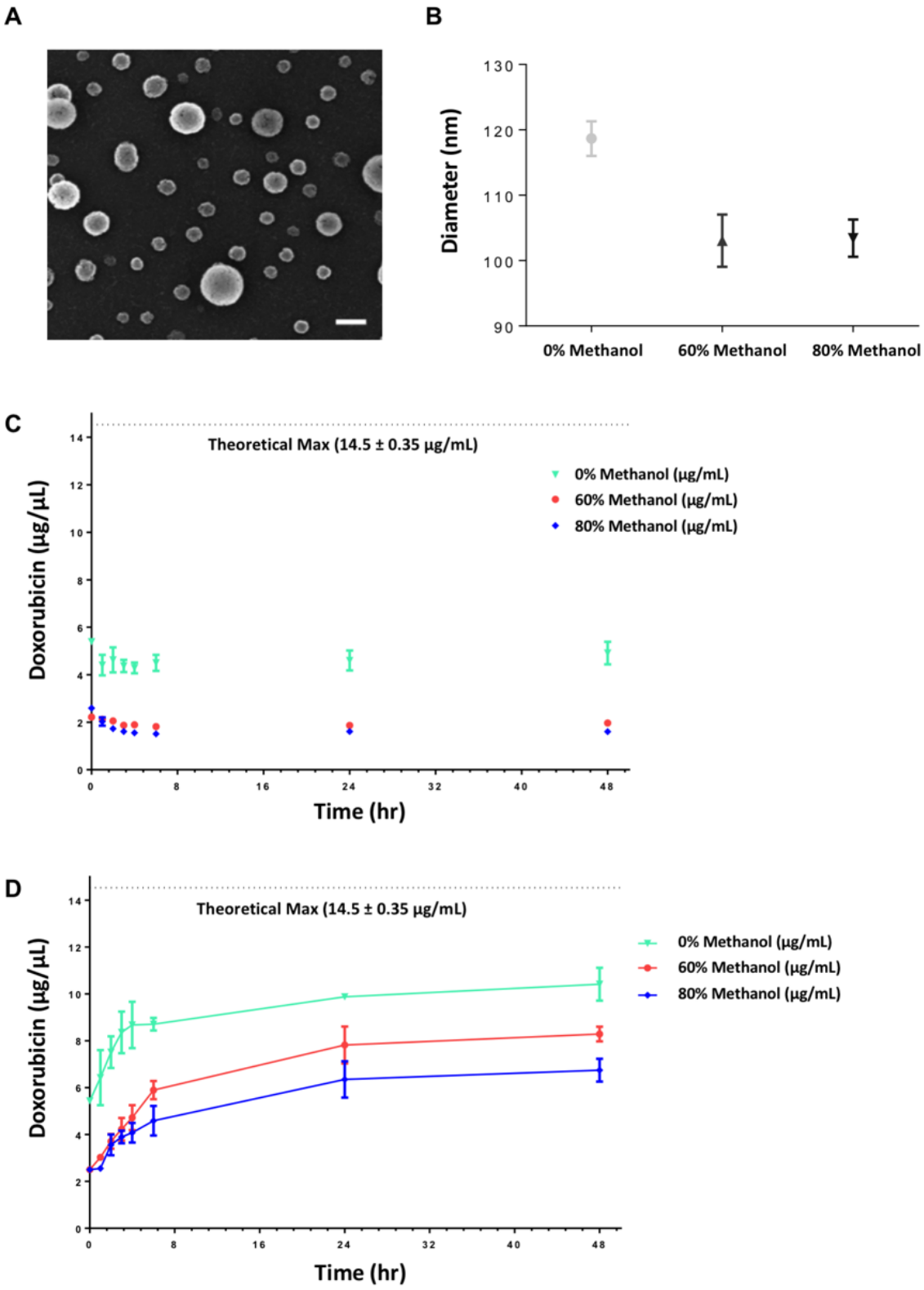

Figure 1. Characterization of Dox-np Size and Effect of Temperature on Doxorubicin Release. (A) Representative scanning electron microscopy images of Dox-np particles. (B) Hydrodynamic diameter of nanoparticles assessed via dynamic light scattering revealed decreasing nanoparticle size with increasing methanol content. Scale bar = 200 nm, n=2. (C) At 4°C, minimal Dox was released in an initial burst at t = 0 hours with no further release over 48 hours. (D) At 37°C, Dox was released from the nanoparticle matrix with an acceleration from t=0-6 hours, followed by a gradual increase until steady state at 24 hours. Dox-np (A80) had a slower rate of release compared to Dox-np (A0), with lower maximum release after 48 hours. As depicted, theoretical maximum release was never achieved. Error bars denote $\chi \pm$ sem. n=2.

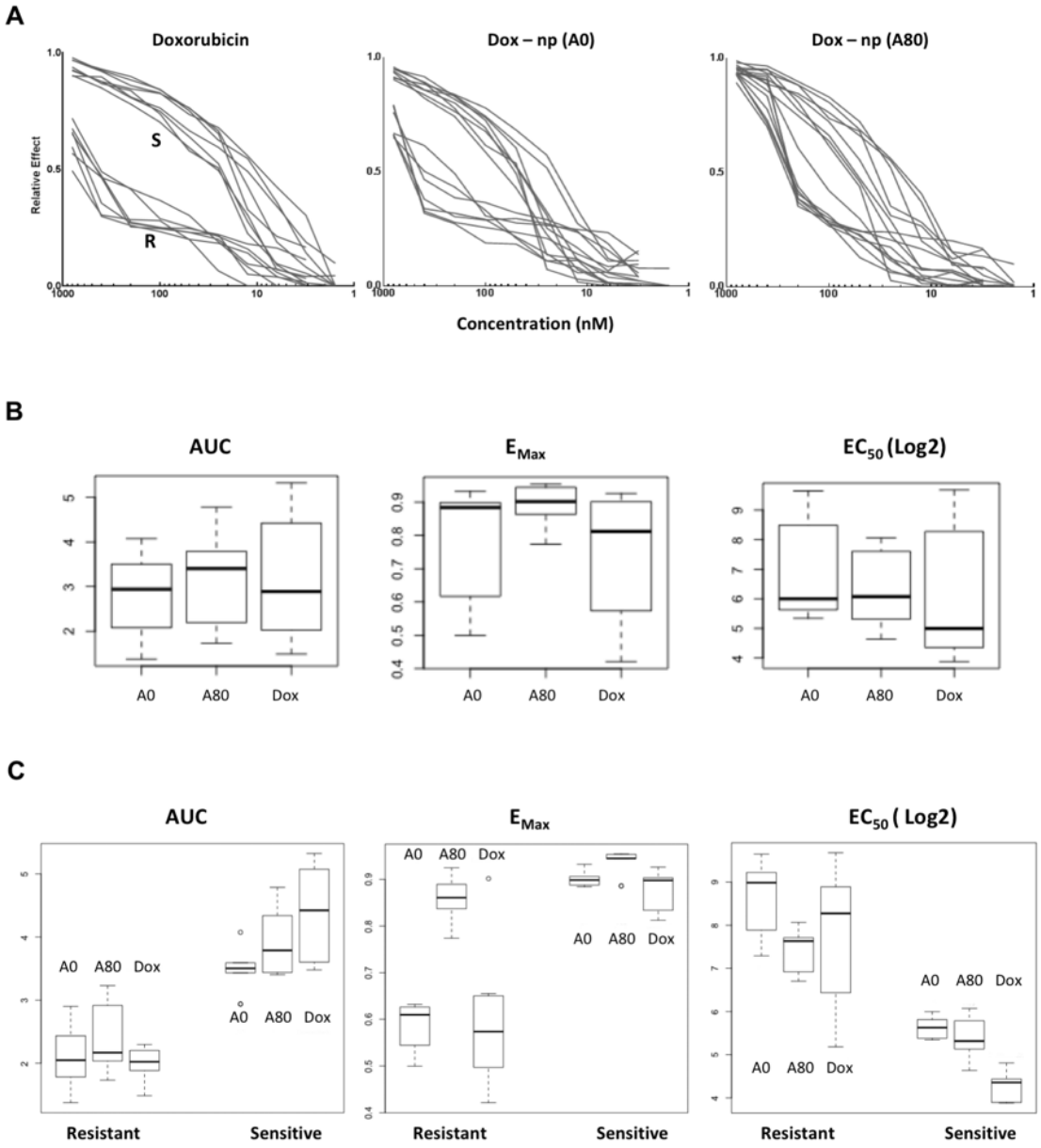

Figure 2. Improved Dose-Response Relationship of Dox-np versus Doxorubicin In Triple-Negative Breast Cancer (TNBC). (A) Dose-response curves representing different variation in dose-response relationships. Patterns of dose-response are shown for Dox, Dox-np (A0) and Dox-np (A80). Each curve represents a dataset for one cell line. High variation was observed for doxorubicin and curves separate into 2 cohorts representing sensitive (S) and resistant (R) lines. This separation was also evident for Dox-np (A0). Dox-np (A80) gave a more uniform distribution. (B) Distribution of dose-response parameters AUC, E_{Max} and EC_{50} for Dox-np (A80) relative to Dox, or Dox-np (A0) across 6 cancer cell lines. Values were computed from sigmoidal dose-response simulations and drawn as box and whisker plots showing median value (black horizontal line) with interquartile range (boxes). Bars extending to 1.5× the interquartile range indicate variance. Among all cell lines, E_{Max} is most improved relative to Dox. (C) Distribution of dose-response parameters segregated according to Dox resistance or sensitivity. Resistant lines were mesenchymal TNBC's (BL2 and M subtype). Dox-np (A80) had statistically significantly superior E_{Max} relative to Dox in the resistant cohort ($P < 0.0001$; Wilcoxon signed rank test) with slightly increased AUC (P=NS) and statistically significantly decreased EC_{50} ($P < 0.005$; Wilcoxon signed rank test), consistent with improved anti-cancer activity overall. Outliers are shown as non-connected data points in the plots.

High variation was observed for Dox such that curves dichotomized according to steep versus shallow slope, demarcating sensitive (S) and resistant (R) cohorts, respectively. This trend was also apparent for Dox-np (A0); however, Dox-np (A80) dose-response curves were steeper in the resistant cohort specifically, generating a more uniform dose-response relationship across all cell

lines (Figure 2A). Dose-response parameters computed from sigmoidal dose-response curves are summarized in Table 2. Median values across all cell lines (black horizontal line) are depicted as box and whisker plots showing interquartile range (boxes) and variance (bars extending to 1.5× the interquartile range (Figure 2B). This analysis indicated increased AUC and E_{Max} for Dox-np (A0 and A80) relative to Dox, although only E_{Max} reached statistical significance ($P < 0.05$; Wilcoxon signed rank test, Dox-np (A80) versus Dox). However, median EC_{50} increased for Dox-np, consistent with decreased sensitivity at doses associated with suppression of proliferation. Thus, improvements in dose-response parameters occurred at the high concentration range.

Table 2: Dose-Response Parameters for Dox versus Dox-np in a Panel of Cancer Cell Lines

		E_{Max}		AUC		EC_{50} (Log_2)	
Tumor Type	***Cell Line***	**Dox**	**Dox-np (A80)**	**Dox**	**Dox-np (A80)**	**Dox**	**Dox-np (A80)**
TNBC-BL2	**Sum149PT**	0.52	0.88	1.99	2.41	5.93	7.36
TNBC-M	**Hs578T**	0.68	0.88	2.01	2.11	8.45	7.66
TNBC-M	**MDA-MB-157**	0.50	0.80	1.92	3.02	9.63	6.92
TNBC-BL1	**MDA-MB-468**	0.89	0.95	5.07	4.33	3.89	5.13
NSCLC	**A549**	0.90	0.95	5.26	5.04	3.42	4.34
Ovarian	**HEY**	0.87	0.93	4.21	3.85	4.37	5.45

Dose-Response modeling enabled computation of metrics across 6 cancer cell lines, including E_{max} (a measure of efficacy), AUC (area under the dose-response curve) and EC_{50} (a measure of potency). Cell lines highlighted in grey represent the resistant cohort and are molecular subtypes of TNBC that are metastatic and have poor overall survival. Dox-np (A80) demonstrated dramatically superior E_{Max} in these cell lines, relative to Dox.

TNBC – Triple negative breast cancer; BL1 – Basal-like 1; BL2 – Basal-like 2; M – Mesenchymal; NSCLC – Non-small cell lung carcinoma.

To facilitate a more nuanced evaluation of sensitive and resistant cohorts, dose-response parameters were recomputed for these 2 groups and box plots redrawn (Figure 2C). Resistant lines (SUM149PT, Hs578T and MDA-MB-157) were BL2 and mesenchymal (M) subtypes of TNBC that represent types of disease with aggressive, metastatic tumor biology (15). Dox-np (A80) had statistically significantly increased E_{Max} relative to Dox in the resistant cohort ($P < 0.001$; Wilcoxon signed rank test) and slightly increased AUC and decreased EC_{50}, consistent with improved anti-tumor activity overall. In the sensitive cohort, Dox had comparable EC_{Max} as Dox-np, while AUC and EC_{50} values showed decreased effect of Dox-np relative to Dox. This lack of sensitization by Dox-np in sensitive cohorts is also shown in dose-response curves for individual cell lines (Figure S1). Thus, Dox-np has superior efficacy specifically in BL2 and M subtypes of TNBC in vitro.

Dox-np Has Superior Tumor Cell Kill in BL2 and M Subtypes of Breast Cancer

High-dose Dox-np (A80) caused enhanced tumor cell kill in chemoresistant TNBC cell lines (Figure 3). Dox was unable to elicit the same degree of tumor cell kill at equivalent concentrations (800nM). At lower doses (100 nM), the difference in survival between Dox and Dox-np was not remarkable, consistent with other data indicating that the superiority of Dox-np is limited to high concentrations.

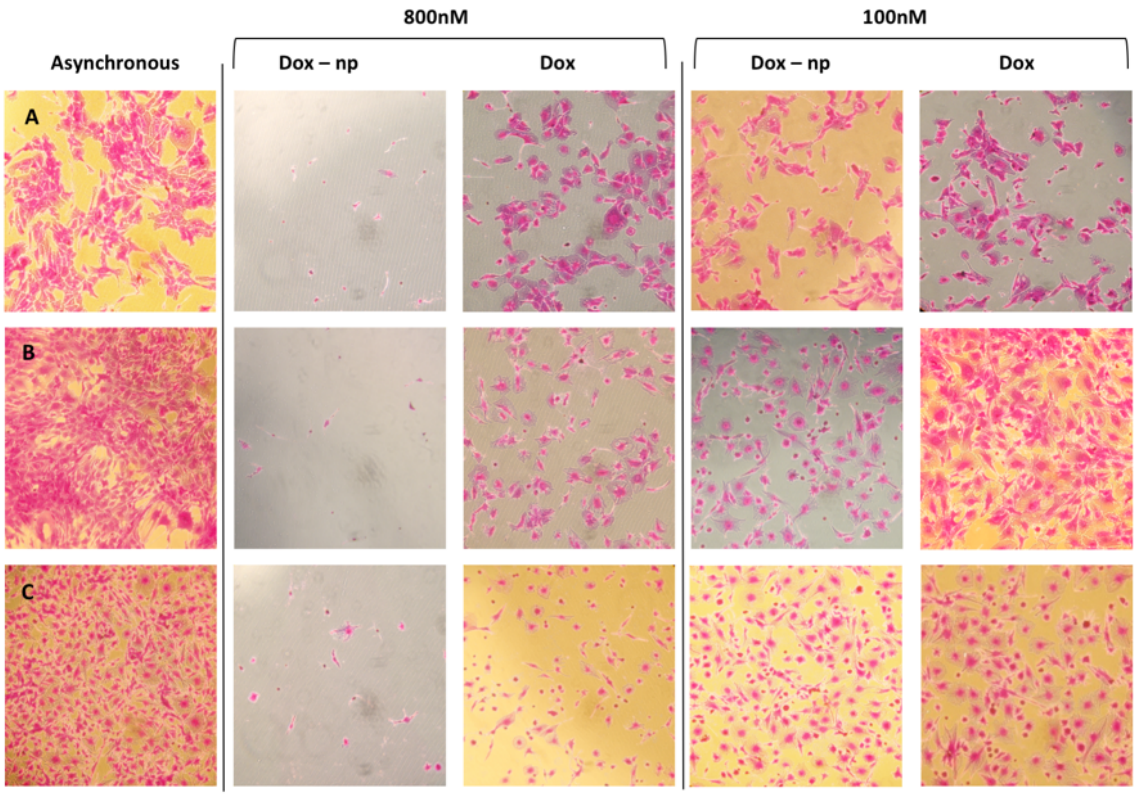

Figure 3. E_{Max} Doses of Dox-np Cause Enhanced Cell Death Relative to Doxorubicin in Chemorefractory Triple-Negative Breast Cancer (TNBC). Surviving TNBC cells in (A) SUM149PT, (B) Hs578T, and (C) MDA-MB-157 following incubation with either Dox-np (A80) or Dox. Representative images were obtained from SRB-stained plates, as described in Materials and Methods (10× magnification).

Increased Endocytosis as a Mechanism for Superior Efficacy of Dox-np

Nanoparticles are thought to be taken into cells via endocytosis (16), although understanding nanoparticle uptake remains a challenge in the field. To address differences in uptake between TNBC subtypes, we used fluorescent beads as a surrogate to monitor Dox-np uptake. Both M type cell lines (Hs578T and MDA-MB-157) incorporated significantly more beads than BL1 and unclassified (UN) subtypes (Table 3 and Figure S2), implying increased endocytosis in Dox-refractory M type TNBC cells. This associates with the superior E_{Max} and high rate of cell death by Dox-np in these cells and could offer mechanistic insight for future studies.

Table 3: Increased Fluorescent Bead Uptake in Mesenchymal Versus Basal TNBC

Histology / Subtype	Cell Line	% Fluorescent Bead Uptake * (Number of beads per cell - range)
BL1	MDA-MB-468	2.5 (1–3)
UN	BT-20	1.5% (1–2)
M	Hs578T	90% (1–15)
M	MDA-MB-157	43% (1–6)

*Bead uptake was quantified by counting 6 fields at 40× magnification and determining the number of cells with red fluorescence as a proportion of the total number of cells (counted by phase). The range of spots per cell are indicated in parentheses. BL1 = basal-like 1; M = mesenchymal; TNBC = triple-negative breast cancer; UN = unclassified.

Discussion

The need to develop and test therapies with superior therapeutic index is a driving force in modern cancer drug development as we advance toward treating cancer as a chronic condition. An exciting advance is the development of nanoparticle technology, exemplified by the clinical success of Doxil and Abraxane. The enthusiasm surrounding nanotechnology centers on the potential to modulate pharmacokinetics to enhance drug delivery and pharmacodynamics, while reducing systemic toxicity. We synthesized a malleable nanoparticle capable of releasing Dox in a time- and dose-regulated manner. A major benefit of nanotechnology such as ours is the ability to customize various elements involved in synthesis, in this case, manipulating initial methanol content, which significantly affected performance parameters including size and release rate and correlated with improved in vitro activity.

Tris-buffered saline possesses amines that block silanol interactions between nanoparticles thereby inhibiting aggregation, which would otherwise impair the EPR effect and diminish ability to accumulate in tumor tissue. Enhanced reduction of individual particle size was achieved by choosing TMOS and methanol as the alkoxide and alcohol, respectively, as each contributes independently to minimization of size (17). Polyethylene glycol (PEG) was incorporated into the body of the nanoparticle as it has been demonstrated that PEG controls the pore size in the sol-gel matrix of our platform and thus is the primary effector of release characteristics (12, 18). As a steric stabilizer, PEG also contributes to maintaining small individual particle size by interfering with inter-particle hydrogen bonding to decrease nanoparticle aggregation (19).

Conclusion

The cellular mechanism that results in improved anti-tumor efficacy of nanoparticle formulations of cytotoxic drugs relative to free drug is multifactorial and includes enhanced permeation and retention (EPR) effects highly dependent on tumor microenvironment, increased uptake into cells via endocytosis, and circumvention of drug transporter activation / recruitment, such as ABC family transporters including Pgp (20, 21). The most impressive anti-tumor property of Dox-np is the potent cell-kill ability in refractory TNBC cell lines representative of disease with unmet clinical need. Thus, these are translationally significant findings that warrant future in vivo evaluation of Dox-np.

Acknowledgments

This work was supported by National Cancer Institute Grant CA077263 and the Breast Cancer Research Foundation. A.J.F. would like to acknowledge the Dermatology Foundation Career Development Awards Program.

Disclosures

A.J.F. and J.M.F. are co-inventors of the nanoparticle platform utilized in the studies described. This technology has been licensed to Zylo Therapeutics for commercial development.

Conflict of Interests

The authors declare no conflicts of interest. For signed statements, please contact the journal office: editor@precisionnanomedicine.com

Quote this article as: Krausz AE, Adler BL, Makdisi J, Schairer D, Rosen J, Landriscina A, Navati M, Alfieri A, Friedman JM, Nosanchuk JD, Rodriguez-Gabin A, Ye KQ, McDaid HM, Friedman AJ, Nanoparticle-Encapsulated Doxorubicin Demonstrates Superior Tumor Cell Kill in Triple Negative Breast Cancer Subtypes Intrinsically Resistant to Doxorubicin, Precis. Nanomed. 2018;1(3):172-185 https:/doi.org/10.33218/prnano1(3).181029.1

References

1. Gonzalez-Angulo AM, McGuire SE, Buchholz TA, Tucker SL, Kuerer HM, Rouzier R, et al. Factors predictive of distant metastases in patients with breast cancer who have a pathologic complete response after neoadjuvant chemotherapy. Journal of clinical oncology : official journal of the American Society of Clinical Oncology. 2005;23(28):7098-104. Epub 2005/09/30. doi: 10.1200/JCO.2005.11.124. PubMed PMID: 16192593.
2. Liedtke C, Mazouni C, Hess KR, Andre F, Tordai A, Mejia JA, et al. Response to neoadjuvant therapy and long-term survival in patients with triple-negative breast cancer. Journal of clinical oncology : official journal of the American Society of Clinical Oncology. 2008;26(8):1275-81. Epub 2008/02/06. doi: 10.1200/JCO.2007.14.4147. PubMed PMID: 18250347.
3. Prat A, Parker JS, Karginova O, Fan C, Livasy C, Herschkowitz JI, et al. Phenotypic and molecular characterization of the claudin-low intrinsic subtype of breast cancer. Breast cancer research : BCR. 2010;12(5):R68. Epub 2010/09/04. doi: 10.1186/bcr2635. PubMed PMID: 20813035; PubMed Central PMCID: PMC3096954.
4. Masuda H, Baggerly KA, Wang Y, Zhang Y, Gonzalez-Angulo AM, Meric-Bernstam F, et al. Differential response to neoadjuvant chemotherapy among 7 triple-negative breast cancer molecular subtypes. Clinical cancer research : an official journal of the American Association for Cancer Research. 2013;19(19):5533-40. Epub 2013/08/21. doi: 10.1158/1078-0432.CCR-13-0799. PubMed PMID: 23948975; PubMed Central PMCID: PMC3813597.
5. Lehmann BD, Jovanović B, Chen X, Estrada MV, Johnson KN, Shyr Y, et al. Refinement of Triple-Negative Breast Cancer Molecular Subtypes: Implications for Neoadjuvant Chemotherapy Selection. PLoS ONE. 2016;11(6):e0157368. doi: 10.1371/journal.pone.0157368.
6. Gref R, Minamitake Y, Peracchia MT, Trubetskoy V, Torchilin V, Langer R. Biodegradable long-circulating polymeric nanospheres. Science. 1994;263(5153):1600-3. Epub 1994/03/18. PubMed PMID: 8128245.
7. Barenholz Y. Doxil(R)--the first FDA-approved nano-drug: lessons learned. Journal of controlled release : official journal of the Controlled Release Society. 2012;160(2):117-34. Epub 2012/04/10. doi: 10.1016/j.jconrel.2012.03.020. PubMed PMID: 22484195.
8. Friedman AJ, Han G, Navati MS, Chacko M, Gunther L, Alfieri A, et al. Sustained release nitric oxide releasing nanoparticles: characterization of a novel delivery platform based on nitrite containing hydrogel/glass composites. Nitric oxide : biology and chemistry / official journal of the Nitric Oxide Society. 2008;19(1):12-20. Epub 2008/05/07. doi: 10.1016/j.niox.2008.04.003. PubMed PMID: 18457680.
9. Gupta R, Kumar A. Bioactive materials for biomedical applications using sol-gel technology. Biomed Mater. 2008;3(3):034005. Epub 2008/08/12. doi: 10.1088/1748-6041/3/3/034005. PubMed PMID: 18689920.
10. Sanchez DA, Schairer D, Tuckman-Vernon C, Chouake J, Kutner A, Makdisi J, et al. Amphotericin B releasing nanoparticle topical treatment of Candida spp. in the setting of a burn wound. Nanomedicine : nanotechnology, biology, and medicine. 2014;10(1):269-77. Epub 2013/06/19. doi: 10.1016/j.nano.2013.06.002. PubMed PMID: 23770066.
11. Han G, Tar M, Kuppam DS, Friedman A, Melman A, Friedman J, et al. Nanoparticles as a novel delivery vehicle for therapeutics targeting erectile dysfunction. The journal of sexual medicine. 2010;7(1 Pt 1):224-33. Epub 2009/09/22. doi: 10.1111/j.1743-6109.2009.01507.x. PubMed PMID: 19765204; PubMed Central PMCID: PMC2864537.
12. Seleem MN, Munusamy P, Ranjan A, Alqublan H, Pickrell G, Sriranganathan N. Silica-antibiotic hybrid nanoparticles for targeting intracellular pathogens. Antimicrobial agents and chemotherapy. 2009;53(10):4270-4. Epub 2009/08/12. doi: 10.1128/AAC.00815-09. PubMed PMID: 19667284; PubMed Central PMCID: PMC2764215.
13. Yuan H, Bao X, Du YZ, You J, Hu FQ. Preparation and evaluation of SiO2-deposited stearic acid-g-chitosan nanoparticles for doxorubicin delivery. International journal of nanomedicine. 2012;7:5119-28. Epub 2012/10/12. doi: 10.2147/IJN.S35575. PubMed PMID: 23055724; PubMed Central PMCID: PMC3463401.

14. Fallahi-Sichani M, Honarnejad S, Heiser LM, Gray JW, Sorger PK. Metrics other than potency reveal systematic variation in responses to cancer drugs. Nat Chem Biol. 2013;9(11):708-14. doi: 10.1038/nchembio.1337. PubMed PMID: 24013279; PubMed Central PMCID: PMCPMC3947796.
15. Lehmann BD, Bauer JA, Chen X, Sanders ME, Chakravarthy AB, Shyr Y, et al. Identification of human triple-negative breast cancer subtypes and preclinical models for selection of targeted therapies. The Journal of clinical investigation. 2011;121(7):2750-67. Epub 2011/06/03. doi: 10.1172/JCI45014. PubMed PMID: 21633166; PubMed Central PMCID: PMC3127435.
16. Moore A, Weissleder R, Bogdanov A, Jr. Uptake of dextran-coated monocrystalline iron oxides in tumor cells and macrophages. Journal of magnetic resonance imaging : JMRI. 1997;7(6):1140-5. Epub 1997/12/24. PubMed PMID: 9400860.
17. Stöber W. Controlled growth of monodisperse silica spheres in the micron size range. J Colloid Interface Sci. 1968;26(1):62-9. doi: 10.1016/0021-9797(68)90272-5.
18. Han G, Friedman A, Friedman J. Nitric Oxide Releasing Nanoparticle Synthesis and Characterization. In: McCarthy HO, Coulter JA, editors. Nitric oxide : biology and chemistry / official journal of the Nitric Oxide Society. Methods in Molecular Biology. 704: Humana Press; 2011. p. 187-95.
19. Xu H, Yan F, Monson EE, Kopelman R. Room-temperature preparation and characterization of poly (ethylene glycol)-coated silica nanoparticles for biomedical applications. Journal of Biomedical Materials Research Part A. 2003;66A(4):870-9. doi: 10.1002/jbm.a.10057.
20. Kirtane AR, Kalscheuer SM, Panyam J. Exploiting nanotechnology to overcome tumor drug resistance: Challenges and opportunities. Advanced drug delivery reviews. 2013;65(13-14):1731-47. Epub 2013/09/17. doi: 10.1016/j.addr.2013.09.001. PubMed PMID: 24036273; PubMed Central PMCID: PMC3849460.
21. El Andaloussi S, Mager I, Breakefield XO, Wood MJA. Extracellular vesicles: biology and emerging therapeutic opportunities. Nat Rev Drug Discov. 2013;12(5):347-57. doi: 10.1038/nrd3978.

Supporting Information

Dynamic Light Scattering (DLS)

A suspension of Dox-np (10 mg/mL) in distilled water was vortexed for 30 seconds to break up nanoparticle aggregates, followed by sonication on ice for 1 minute. The nanoparticle size distribution profile was assessed using DynaPro NanoStar (Wyatt Technology, Santa Barbara, CA). All readings were executed in triplicate and compiled with an acquisition length of 5 seconds and a total of 40 acquisition attempts. Average particle hydrodynamic diameter was calculated from the results.

Scanning Electron Microscopy (SEM)

Nanoparticles were plated on poly-L-lysine-coated coverslips, critical point dried using liquid CO_2 in a Samdri-795 Critical Point Dryer (Tousimis, Rockville, MD), and sputter coated with chromium in a Q150T ES Sputter Coater (Quorum Technologies Ltd, East Sussex, UK). Samples were examined under a Supra Field Emission Scanning Electron Microscope (Carl Zeiss Microscopy, Peabody, MA) with accelerating voltage of 3 kV.

Maximum Encapsulation of Dox

The theoretical maximum of Dox encapsulated within Dox-np was calculated using the weight of doxorubicin used in synthesis and the total weight of the synthesized nanoparticles, such that: Theoretical maximum = (Total doxorubicin used in synthesis / Total weight of synthesized np)/(weight of np used in release experiment/ volume of solvent used in experiment). Dox-np variants were suspended in dimethyl sulfoxide (DMSO) at concentrations with maximum theoretical yields of either 0.32 mM or 0.08 mM (12 mg nanoparticle/mL = 0.32 mM maximum theoretical yield). The samples were agitated at 37°C for 24 hours and then pelleted at 13.2k rpm for 5 minutes. In order to quantify the concentration of nano-encapsulated Dox in Dox-np, a reference sample of 2 mg/ml of Dox was obtained and diluted to 0.08 mM in DMSO. Spectrophotometric analysis of the standard showed an absorption peak at 481 nm. The absorption value at this wavelength was used to calculate an absorption coefficient for Dox in DMSO. The supernatant from each Dox-np sample was measured and the concentration of Dox then calculated.

In Vitro Release kinetics

The intrinsic fluorescence of Dox was utilized to analyze the release characteristics of the Dox-np variants via spectrophotometry (Thermo Scientific, Waltham, MA). Individual aliquots of 10 mg/ml Dox-np dispersed in phosphate buffered saline (PBS, pH=7.4) were incubated on a rotator at 4 $^{\circ}$C or 37 $^{\circ}$C for a total of 48 h. At various time points, aliquots were pelleted for 5 minutes at 13.2k rpm and the supernatant analyzed using UV-Vis Spectrophotometer. Spectrophotometer settings utilized for Dox were as follows: wavelength = 488 nm, extinction coefficient = 11500 1/(M-cm), atomic mass = 543.52.

Cell Culture

The cancer cell lines A549 (human lung adenocarcinoma), HEY (human ovarian adenocarcinoma), MD-MB-157, Hs578T and MDA-MB-468 (all human TNBC) were purchased from American Type Culture Collection (ATCC; Manassas, VA) and cultured according to ATCC instructions. BRCA mutant SUM149PT cells were obtained from Steve Ethier, University of Michigan. Only early passage cells (5-15) were used in experiments. Cells were authenticated by short tandem repeat profiling before use.

Cell Proliferation Assays

A sulforhodamine B (SRB) colorimetric assay was used to screen for anti-tumor efficacy of Dox compared to Dox-np (S1). Briefly, cells were seeded into 96-well plates at densities ranging from 900-1500 cells per well, and allowed to attach for 24 hours. Six replicate wells were incubated with 800 nM of Dox-np variants, clinical grade Dox and control-np, and 2-fold serial dilutions were made for a total of 9 evaluable doses per treatment. Cells were incubated for 3 cell doublings (3-5 days), after which, adherent cells were fixed with 10% trichloroacetic acid (TCA), washed 5 times with distilled water and stained with 0.4% SRB in 1% acetic acid for 10 minutes. Plates were washed 3 times with 0.1% acetic acid, air-dried, photographed and solubilized in 100 µl unbuffered 10 mM Tris solution (pH 10). Optical

densities at 564 nm (OD_{564}) were obtained and drug effect across multiple doses was calculated as % of vehicle-only control. Experiments were repeated a minimum of 3 times.

Multiparameter Dose-Response Modeling

Dose-response curves for clinical grade Dox and Dox-np were generated by fitting values to a logistical sigmoidal model using nonlinear least-squares regression in the R statistical software suite (http://www.R-project.org/)(S2). Dose-response components, namely E_{Max}, AUC and EC_{50}, were computed and used to describe features of dose-response relationships and to provide a robust comparison of profiles of Dox-np versus Dox. Data were presented as box - whisker plots showing median (horizontal line) and interquartile range (boxes). The advantage of the multiparameter method is to circumvent over-reliance on EC_{50}, otherwise known as potency, which typically describes a concentration corresponding to the half-maximal effect associated with proliferative arrest. Over-reliance on potency fails to account for more clinically relevant features of the dose-response relationship, such as E_{Max}, a measure of efficacy that correlates well with concentrations that cause tumor cell death, and AUC, a metric that combines potency and efficacy into one. Assays were done over 3 cell doublings to minimize concerns that efficacy would be skewed by the rate of cell division (S3).

Fluorescent Bead Uptake

Log-phase growth cancer cells seeded in glass-bottomed plates were incubated in serum-free Dulbecco's modified Eagle's medium supplemented with L-glutamine containing red fluorescent latex beads (0.5 μm mean particle size - L3020, Sigma-Aldrich, St. Louis, Missouri, United States) for 1 hour. Cells were washed 4× in warm PBS containing 0.4% trypan blue to quench extracellular fluorescence, and then fixed in 4% paraformaldehyde in PBS for 20 minutes at room temperature. Cells were washed a further 2× in cold PBS before imaging fluorescent bead uptake. Six fields were imaged at 40× magnification corresponding to 190-550 cells, depending on the cell line. Bead uptake was calculated as the number of cells containing fluorescent beads as a percentage of the total number of cells imaged (by phase contrast). The range in bead uptake per cell line was also determined.

Statistical Analysis

Statistical analyses were performed using GraphPad Prism software (GraphPad Software, Inc., La Jolla, CA), unless otherwise stated. Differences in a given dose-response parameter between Dox-np versus Dox were analyzed using a nonparametric Wilcoxon signed rank test. A *P*-value <0.05 was considered statistically significant in all cases. Data presented reflect a composite analysis of at least 3 independent experiments.

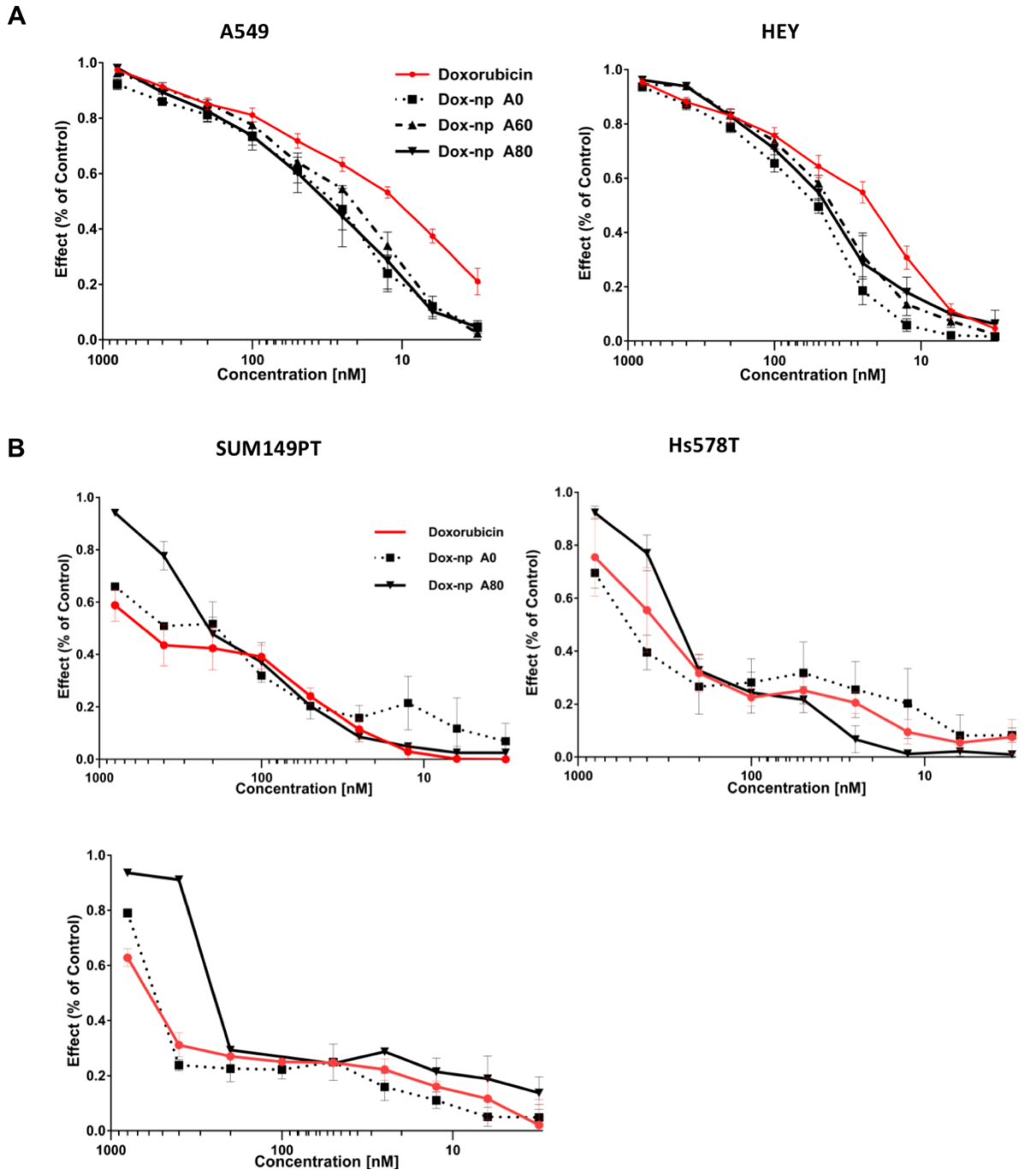

Figure S1: Dose-Response Curves of Dox-np in Cancer Cell Lines. Cells were incubated with the indicated range of drug concentrations for 3 cell doublings. Data shown are mean effect (SRB) relative to vehicle-only control wells ± SEM, n = 3. (A) Dose-response curves for Dox-np (A0, A60 and A80) relative to doxorubicin (red) in chemosensitive cell lines - NSCLC cells, A549 and ovarian carcinoma cells, HEY. (B) Dose-response curves for Dox-np (A0 and A80) relative to doxorubicin (red) in chemoresistant triple-negative breast cancer cell lines – SUM149PT, Hs578T and MDA-MB-157.

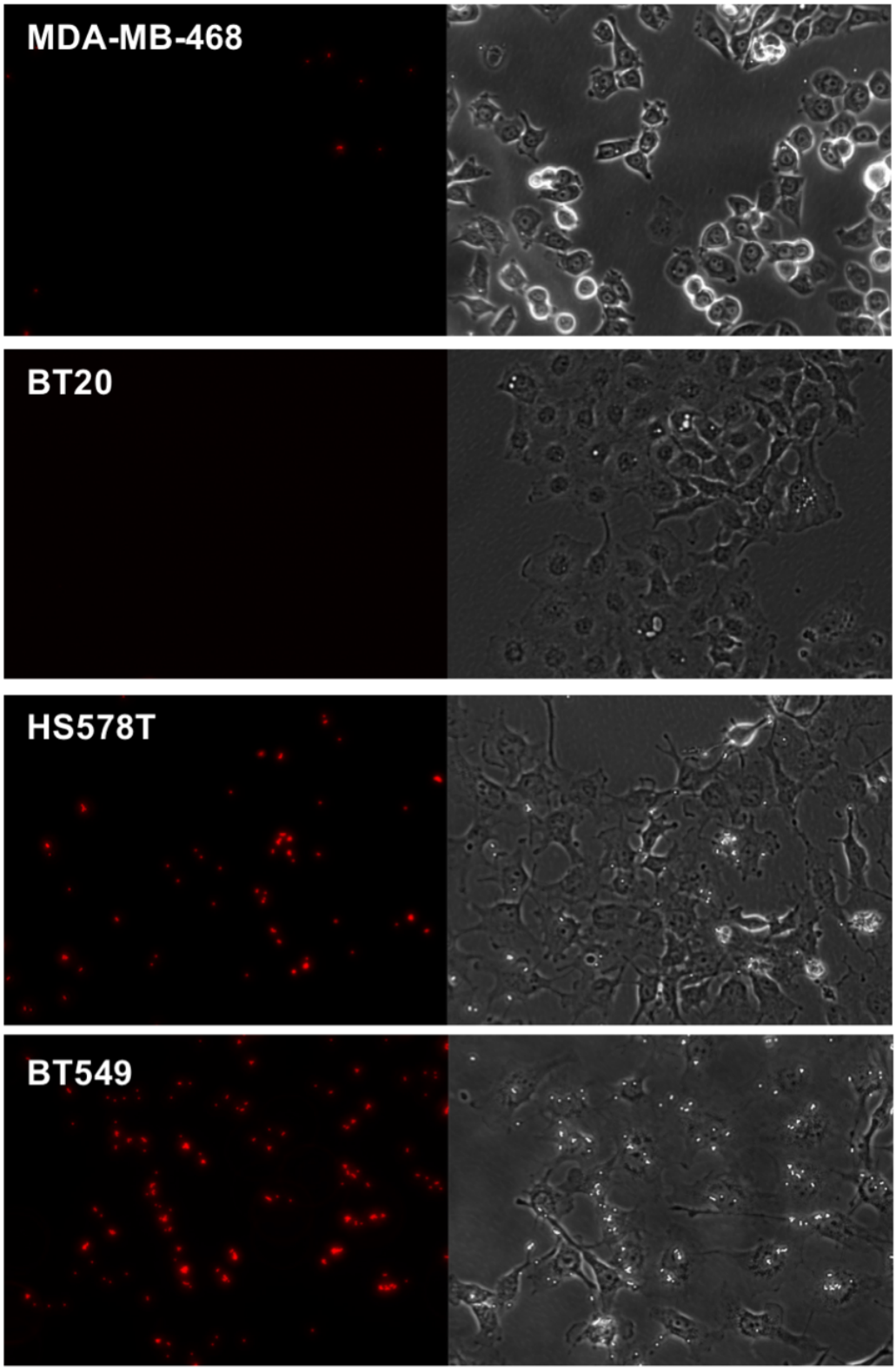

Figure S2 – Enhanced Fluorescent Bead Uptake in Mesenchymal versus Basal Breast Cancer Cells. Cells were incubated with fluorescent beads (0.5um) as described in Materials and Method, and % incorporation determined by counting the number of cells with red fluorescence (left) as a proportion of total cells (right). The chemosensitive cells MDA-MB-468 and BT-20 had minimal bead uptake while both mesenchymal subtypes, Hs578t and BT549 had comparatively higher % uptake.

S1. Voigt W. Sulforhodamine B assay and chemosensitivity. Methods Mol Med. 2005;110:39-48. Epub 2005/05/20. doi: 10.1385/1-59259-869-2:039. PubMed PMID: 15901925.
S2. Fallahi-Sichani M, Honarnejad S, Heiser LM, Gray JW, Sorger PK. Metrics other than potency reveal systematic variation in responses to cancer drugs. Nat Chem Biol. 2013;9(11):708-14. doi: 10.1038/nchembio.1337. PubMed PMID: 24013279; PubMed Central PMCID: PMCPMC3947796.
S3. Hafner M, Niepel M, Chung M, Sorger PK. Growth rate inhibition metrics correct for confounders in measuring sensitivity to cancer drugs. Nat Methods. 2016;13(6):521-7. doi: 10.1038/nmeth.3853. PubMed PMID: 27135972; PubMed Central PMCID: PMCPMC4887336.